RSC Advances

PAPER

View Article Online
View Journal | View Issue

Cite this: *RSC Adv.*, 2024, **14**, 33019

Microwave-driven oleic acid esterification over chlorosulfonic acid-treated hydroxyapatite: synergism for intensified biodiesel production

Boutaina Rezki, *[a] Younes Essamlali,[b] Othmane Amadine,[b] Said Sair,[b] Mina Aadil[a] and Mohamed Zahouily[ab]

Treating hydroxyapatite (HAP) with sulfonic acid without structural destruction remains challenging owing to the sensitivity of HAP to acidic pH. In this work, natural derived HAP was prepared using natural phosphate *via* a dissolution/precipitation process. Notwithstanding the challenge, the prepared HAP was treated with three concentrations of chlorosulfonic acid in dichloromethane to prepare HAP-S1, HAP-S2 and HAP-S3 depending on the acid content under carefully controlled conditions. The treatment of HAP with the lowest acid concentration led to the preservation of the apatite framework with surface modification of sulfonic acid groups. As the acid concentration increased, HAP, $CaHPO_4$ and $CaSO_4$ were obtained. A further increase in the acid concentration led to the formation of $CaSO_4$ with the coexistence of $Ca(H_2PO_4)_2 \cdot H_2O$. Subsequently, the catalytic activity of HAP-S1 was evaluated in oleic acid esterification under microwave irradiation, resulting in a yield of up to 87% under optimized conditions of 10 wt% of catalyst to oleic acid weight, 10 : 1 methanol to oleic acid molar ratio, and 40 min reaction duration under microwave irradiation at 150 °C. The activity of HAP-S1 was attributed to the active S=O and S–O–H functional groups, and a possible mechanism of acid-catalyzed esterification is proposed. The catalyst was also tested in the transesterification reaction of rapeseed oil, achieving a conversion of 40.2% after 60 min reaction duration under microwave irradiation. Furthermore, the catalyst was evaluated in a two-step esterification reaction to investigate its activity towards acidified feedstocks. Results showed that after two successive runs, acidity was reduced by 79.6% with a total FAME yield of 40.13%. The obtained results indicate that this catalyst, being an acid catalyst, is more suitable for direct esterification.

Received 12th August 2024
Accepted 29th September 2024

DOI: 10.1039/d4ra05862c

rsc.li/rsc-advances

1. Introduction

Acid catalysis is one of the most important areas of catalysis science. Typically, Lewis or Brønsted acid catalysts are responsible for the processing of important transformations such as Fischer esterification.[1] In particular, the esterification reaction of fatty acids such as oleic acids (OA) and palm fatty acid distillate (PFAD) with methanol has attracted significant interest because the obtained monoalkyl esters have similar physicochemical properties to those of petrodiesel.[2,3] Monoalkyl esters, namely, biodiesel, can be blended with conventional diesel and used in engines without further modification.[4,5] Generally, the esterification of fatty acids is carried out using homogeneous acid catalysts such as H_2SO_4, H_3PO_4, HCl, and *p*-toluenesulfonic acid, where the proton (H^+) is the acid moiety, according to the Brønsted–Lowry acid–base theory.[6] However, although homogeneous catalysts provide high ester yields under mild conditions, they are corrosive to reactors, and further neutralization steps are required to purify the final product. Therefore, to facilitate the separation and regeneration steps, many solid catalysts have been investigated in esterification such as sulfated metal oxides,[7] sulfonated mixed metal oxides,[8] sulfonic acid-functionalized mesoporous carbon materials or silicas,[9] heteropolyacids,[10] polyoxometalates,[11] TiO_2/NP[12] and acid-derived apatite catalysts.[13,14] It should be noted that biodiesel can be obtained by adopting different processes depending on the acidity of feedstocks and the type of catalysts.[15] In general, biodiesel can be produced *via* direct base-catalyzed transesterification of oils.[16,17] Moreover, it is obtained from highly acidic feedstocks by a simultaneous esterification/transesterification process using bifunctional or strong acid catalysts.[18] It is also produced by a two-step esterification and transesterification process by reducing the acidity of the initial feedstock *via* esterification to make it suitable for the transesterification reaction.[19]

[a]*Faculty of Sciences and Technology, Laboratory of Materials, Catalysis and Natural Resources Valorization, Hassan II University of Casablanca, 20650, Mohammedia, Casablanca-Settat, Morocco. E-mail: boutainachimie@gmail.com; boutaina.rezki@etu.fstm.ac.ma*

[b]*Moroccan Foundation for Advance Science Innovation and Research, VARENA Center, Mohammed VI Polytechnic University, Ben Guerir, Morocco*

Hydroxyapatite (HAP) is an attractive inorganic compound due to its flexible framework, which can accept many partial cationic and anionic substitutions, and also due to its excellent surface activity related to its possible functionalization.[20,21] In this context, the surface modification of HAP has received significant interest in acid-catalyzed transformations.[22–24] For example, supported synthetic apatite with sulfonic acid groups (HAP-SO_3H) provided new strong catalytic acid sites for condensation and cyclization between amidoxime and aldehyde, as reported by El Mansouri *et al.*[22] In addition, magnetic sulfonated hydroxyapatite-encapsulated-γ-Fe_2O_3 has been widely used in many acid-catalyzed reactions, for example, it was found to exhibit a good performance in the N-formylation of amines, as detailed by Ma'mani *et al.*[25–28] Furthermore, HAP-$AEPH_2$-SO_3H was found to be an efficient catalyst for the esterification of carboxylic acids with alcohols, as reported by Siavashi *et al.*[29] Although many solid catalysts have been employed for biodiesel production, apatite-based catalysts have recently attracted attention due to their effectiveness in promoting the synthesis of biodiesel from diverse feedstocks.[21] Herein, it is essential to highlight that the utilization of apatite-derived catalysts aligns with the sustainable catalysis principles. This relies on utilizing materials with high natural abundance to produce high-value chemicals in an environmentally sustainable approach. In this context and motivated by the abundance of phosphate mineral in Morocco, the main objective of the present study is the preparation of an acidic catalyst based on natural hydroxyapatite modified with sulfonic acid and its application in biodiesel production through the oleic acid esterification reaction as a model reaction.

Alternatively, thermo-catalytic conversions occur in heated reactors using various heating modes (conventional oil-bath reflux heating, electrical heating, and microwave-assisted heating). The use of microwave irradiation for the synthesis of biodiesel significantly reduces the time needed for the optimal conversion and produces a higher yield compared to conventional methods.[30] Due to its unique thermal effects, when applying microwave frequencies, microwaves directly heat the internal sample *via* dielectric heating. The polar molecules in reaction medium align with the electromagnetic field, generating heat through molecular rotation, friction, and collision.[31] In contrast, conventional heating, which transfers heat through conduction and convection, may lead to uneven temperature and thermal gradients.[32]

Herein, in the presented research, natural hydroxyapatite was obtained by the dissolution–precipitation process of natural phosphate, and then the obtained liquid phase was precipitated using a highly basic solution. Subsequently, the obtained hydroxyapatite was subjected to a series of treatments with chlorosulfonic acid ($ClSO_3H$) in dichloromethane (DCM). To the best of our knowledge, this is the first report studying the effect of the concentration sulfonic acid in DCM on the structure of natural hydroxyapatite by various characterization techniques. Then, the sulfonated hydroxyapatite (HAP-S1) was utilized in oleic acid esterification with methanol under microwave irradiation. Other tests, such as the transesterification of rapeseed oil and the two-step esterification–transesterification process, were carried out to investigate the activity and selectivity of the catalyst towards the synthesis of biodiesel from different feedstocks. Herein, in this work, and despite the challenges of the deactivation and short-term stability of the catalysts, the acid-based-apatite catalysts are shown to be a promising alternative to other catalysts due to their abundance, easy accessibility and cost-effectiveness. Thus, further research should be conducted to propose better modifications of apatite to realize long-term stability.

2. Material preparation and characterization

2.1. Materials and reagents

Natural phosphorus rock was obtained from Moroccan sedimentary phosphate deposits at mines in the Khouribga region. Oleic acid (technical grade, 90%) was provided by Alfa Aesar. Rapeseed oil was purchased from a local company in the city of Mohammedia, Morocco. Ammonium hydroxide (NH_4OH) (28–30%), nitric acid (HNO_3) (65–67%), phenolphthalein ($C_{20}H_{14}O_4$) and potassium hydroxide (KOH) were purchased from Aldrich Company. Methanol (CH_3OH), ethanol (C_2H_5OH), diethyl ether ($(C_2H_5)_2O$, dichloromethane (CH_2Cl_2) and chlorosulfonic acid ($ClSO_3H$) were all analytical grade and used as received without further purification.

2.2. Materials preparation

2.2.1. Preparation of hydroxyapatite. Hydroxyapatite was prepared *via* the dissolution/precipitation of natural Moroccan phosphate (Fig. 1), inspired by El Asri *et al.*[33] Briefly, 30 g NP was dissolved in concentrated HNO_3 (5 M, 500 mL) solution overnight at room temperature under magnetic stirring. The resulting suspension was centrifuged to remove insoluble impurities such as SiO_2. The collected filtrate containing Ca^{2+} and H_3PO_4 was precipitated with an adequate volume of NH_4OH (30%) solution to adjust the pH of the solution from acidic to base (10–11), which was added dropwise to control the pH. The resulting precipitated was stirred overnight at 85 °C. The resulting white precipitate was collected by centrifugation, washed with distilled water to neutral pH, dried, and calcined at 550 °C for 4 h. The general process for the preparation of HAP from natural phosphate is shown in Fig. 1.

2.2.2. Treatment of hydroxyapatite with $ClSO_3H$. Sulfonic acid treatment of the prepared HAP was performed using three different amounts of $ClSO_3H$ (0.18, 0.25 and 0.45 mL) in 30 mL of DCM, and the prepared solutions had concentrations of 0.089 mol L^{-1}, 0.124 mol L^{-1} and 0.22 mol L^{-1} to obtain HAP-S1, HAP-S2, and HAP-S3 materials, respectively. The sulfonic acid/DCM solution was carefully poured in a burette, and then was added dropwise (at the lowest flow) to a stirred suspension of HAP (1 g) in 30 mL of DCM placed in an ice bath. After 20 min the suspension was centrifuged, vigorously washed with DCM to remove excess acid, and dried at 70 °C prior to use. It should be noted that persons handling chlorosulfonic acid should work in a well-ventilated lab hood, avoid contact with their skin, eyes, and clothing and avoid inhaling vapors. The preparation of these materials was realized many times to ensure reproducibility.

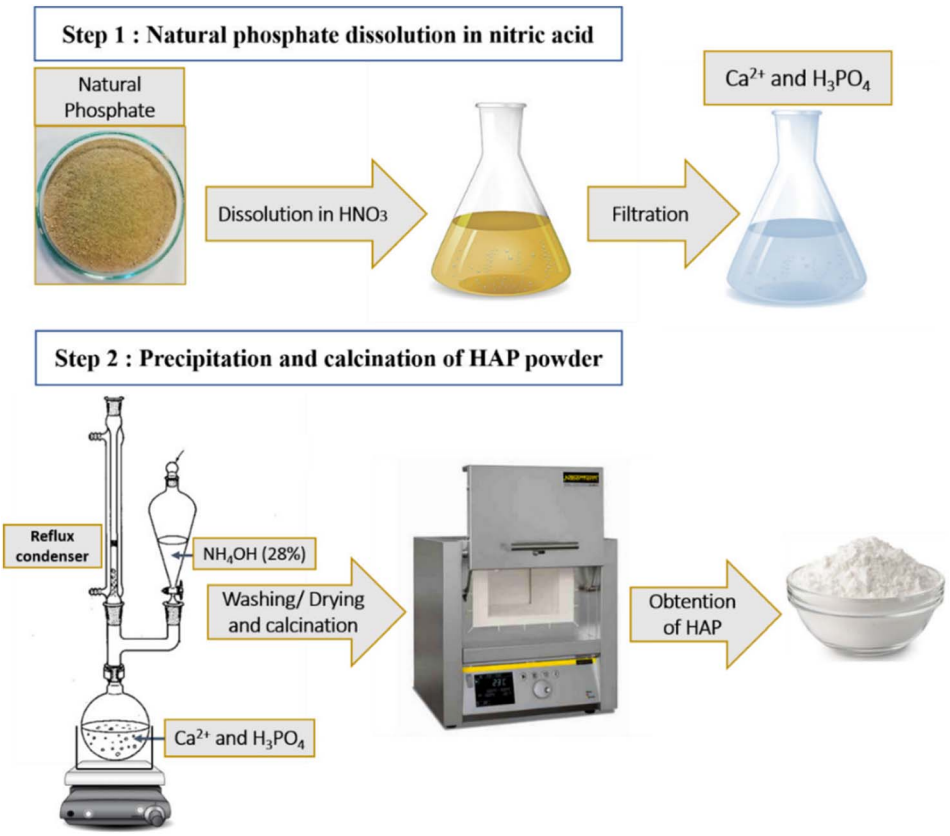

Fig. 1 Hydroxyapatite preparation from the dissolution/precipitation of natural phosphate.

2.3. Material characterization

The X-ray diffraction (XRD) data of the prepared materials were collected at room temperature using a D2 PHASER diffractometer, with the Bragg–Brentano geometry, using CuKa radiation ($\lambda = 1.5406$ Å) at 30 kV and 10 mA. The patterns were scanned in steps of 0.02° (2θ). The Fourier transform infrared (FT-IR) spectra of the samples were obtained using a Bruker Vector 22 spectrometer in the range of 4000–500 cm^{-1} at a resolution of 16 cm^{-1}. Scanning electron microscopy (SEM), energy-dispersive X-ray spectroscopy (EDX) and elemental mapping analysis were performed using a Tecnai G2 microscope at 120 kV. Solid-state ^{31}P nuclear magnetic resonance experiments were performed on a Bruker Advance 600 MHz spectrometer, where powder samples were packed into 4 mm zirconia magic-angle spinning (MAS) rotors and spun at a rotation frequency of 10 kHz. The ^{31}P CP MAS spectra were obtained using the standard cross-polarisation pulse technique followed by ^{1}H high-power decoupling.

2.4. Reaction procedure

The feedstocks in this study, namely, oleic acid and refined rapeseed oil, were utilized without any pretreatment or preheating.

2.4.1. Oleic acid esterification procedure. The esterification of oleic acid was carried out in a 100 mL closed glass vessel (high-pressure vessels) using a microwave irradiation oven (Milestone flexiWAVE). Oleic acid, methanol and catalyst were introduced, mixed and irradiated. A series of reactions was carried out under different operating conditions to determine the optimal conditions for the optimal conversion, as follows: reaction temperature in the range of 100–150 °C, molar ratio of methanol to OA in the range of 6–12, amount of catalyst in the range of 5–12 wt% to weight of OA, and a reaction time in the range of 10 to 60 min. The temperature in the closed vessel was monitored by an infrared (IR) sensor. Upon completion of the reaction, the system was gradually cooled to a temperature below 50 °C. Subsequently, the catalyst was separated by centrifugation at 4500 rpm, and then washed with ethanol, dried at 80 °C and conserved for further reutilization tests. Excess methanol and water generated during the reaction were removed by rotary evaporation under reduced pressure. The conversion percentage of oleic acid to its corresponding ester was determined by calculating the acid value (AV) before and after the reaction using acid–base titration with ethanolic potassium hydroxide solution following eqn (1) and (2), as follows:

$$\mathrm{AV} = \frac{C_{\mathrm{KOH}}\left(V_{\mathrm{eq}} - V_{\mathrm{ref}}\right) \times 56.11}{m} \quad (1)$$

where C_{KOH} is the utilized concentration of ethanolic KOH, V_{eq} is the volume at equilibrium, V_{ref} is the volume of the reference and m is the mass of the sample dissolved in diethyl ether. The conversion calculation was done as follows:

$$C(\%) = \frac{AV_i - AV_f}{AV_i} \times 100 \quad (2)$$

where C is the percent conversion of oleic acid and AV_i and AV_f represent the initial and final acid values of the reaction mixture, respectively. All experiments were conducted in triplicate. The reported conversion results represent the averages of the three experimental results.

In addition, the oleic acid conversion (wt%) under the optimal conditions was also performed using ^{1}H-NMR adopting the following equations:

$$\text{Acid content}(\%) = \frac{A(\alpha\text{-CH}_2) \text{ of carboxylic acid peak}}{\sum A(\alpha\text{-CH}_2) \text{ of carboxylic acid and ester peaks}} \times 100$$

$$\text{Acid conversion } (\%) = [100 - \text{acid content } (\%)]$$

where A is the area under the α-CH_2 triplet.

2.4.2. Transesterification of rapeseed oil. The utilized rapeseed oil had an acid value that is less than 1 mg KOH per g. The transesterification reaction of rapeseed oil was carried out according to the defined optimized conditions of the oleic acid esterification (10 wt% of the catalyst to oil weight, 10 : 1 methanol to oleic acid molar ratio, temperature of 150 °C) for both 40 min and 60 min. At the end of the reaction, the catalyst was removed by centrifugation. Subsequently, the liquid mixture was subjected to rotary evaporation to remove the excess methanol. The separated ester phase was analysed by nuclear magnetic resonance (^{1}H-NMR, Bruker Avance 600 MHz) using deuterated chloroform ($CDCl_3$) as the solvent and tetramethylsilane (TMS) as the internal standard. The oil conversion was calculated using the method reported by Liza *et al.*[34]

2.5. Catalyst characterization

2.5.1. X-ray diffraction. The X-ray diffraction patterns of the pristine and treated hydroxyapatite are presented in Fig. 2. The diffractogram of the prepared HAP is in good agreement with the standard data for the hexagonal structure of pure apatite (JCPDS card 01-074-0565), as indexed by the main typical planes of (002), (211), (300), (202), (310), (222), (213) and (004).[35] After the first treatment with DCM containing chlorosulfonic acid solution, the peaks of the apatite phase were detected for the HAP-S1 material. However, this treatment was accompanied by a slight modification of the intensities and a decrease in the lattice parameters and cell volume compared to that of pure HAP, as shown in Table 1. Upon increasing the concentration of the chlorosulfonic acid solution, the XRD pattern of HAP-S2 showed the presence of the typical HAP peaks and additional intense peaks at $2\theta = 22.4°$ and 30.1° related to the presence of acidic monetite ($CaHPO_4$) according to JCPDS card (01-089-5969) as a result of the partial dissolution process of the hydroxyapatite network in acidic medium, as described by Dorozhkin.[36] In addition, new peaks at $2\theta = 25.4°$ and 32.4° related to the presence of the orthorhombic anhydrite β-$CaSO_4$ phase were also detected according to the JCPDS card (01-072-0916).[37] After high-acidic treatment of HAP, the relative XRD pattern of HAP-S3 showed intense characteristic peaks of β-$CaSO_4$ at $2\theta = 25.4$ and 32.4°, which are related to the formation of anhydrite $CaSO_4$ crystals as a major component, with the presence of tiny peaks related to the existence of residual $Ca(H_2PO_4)_2 \cdot H_2O$ triclinic phase.

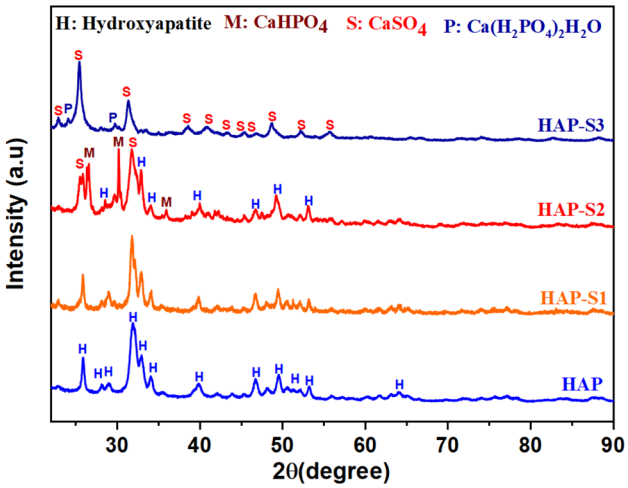

Fig. 2 XRD patterns of the prepared materials.

2.5.2. FTIR spectroscopy. The FTIR analysis results showed the characteristic vibrational bands of the apatite structure for the prepared HAP sample. The bands at 560 and 606 cm^{-1} are assigned to the antisymmetric deformation of the O–P–O groups. The peaks at 960, 1025 and 1090 cm^{-1} are attributed to the symmetric and asymmetric stretching vibration modes of the PO_4^{3-} groups.[19] As shown in Fig. 3, in the spectrum of HAP-S1, additional peaks were observed after the sulfonation of hydroxyapatite, which are related to the asymmetric and symmetric stretching frequencies of S=O of the sulfonic group (SO_3H) at 1350–1342 cm^{-1}, confirming that the SO_3H groups were anchored to HAP framework.[38] Furthermore, a new band appeared at 3600–3036 cm^{-1}, which was attributed to the OH groups that appeared after sulfonation.[38] An additional tiny peak at 888 cm^{-1} attributed to the presence of HPO_4^{2-} ions appeared in the spectrum of HAP-S1, which can be explained by the possible partial transformation of the surface PO_4^{3-} groups into HPO_4^{2-}, as detailed by Dorozhkin.[36,39] A further increase in the acid concentration treatment led to the appearance of the symmetric and asymmetric stretching vibrations of SO_4^{2-} at 670 and 482 cm^{-1} in the spectrum of HAP-S2, respectively.[40] In addition, the intensity of the peaks in the 1000–1130 cm^{-1}

Table 1 Lattice parameters and cell volume of HAP and HAP-S1

Material	Lattice parameters			Volume (Å^3)
	a (Å)	b (Å)	c (Å)	
HAP	9.42779	9.42779	6.8975	530.57
HAP-S1	9.41393	9.41393	6.88259	528.23

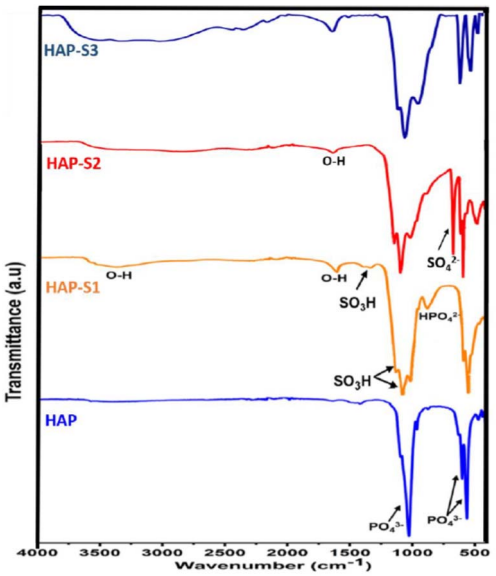

Fig. 3 FT-IR analysis of the prepared materials.

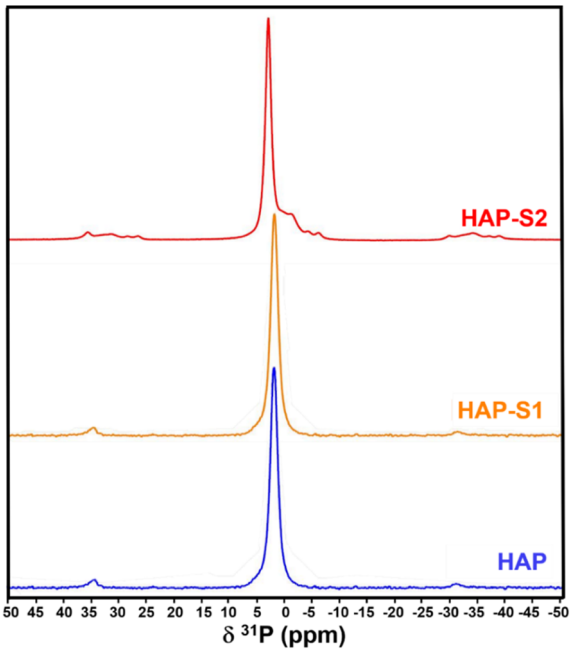

Fig. 4 ^{31}P-MAS-NMR spectra of the prepared samples.

increased due to the coexistence of SO_4^{2-} bands, which overlapped with the vibrational modes of the PO_4^{3-} groups, as reported by Oulguidoum *et al.*[41] In the case of HAP-S3, the characteristic peaks at 670 and 482 cm^{-1} are related to the presence of the SO_4^{2-} groups. The other characteristic peaks of the monocalcium phosphate monohydrate (MCPM) groups may overlap with the characteristic $CaSO_4$ groups. For example, the fundamental vibrational bending and stretching modes of O–P–O, P–O, in-plane P–O–H and out-of-plane P–O–H can be observed in the region of 450–600, 900–1100, 1200–1250, and 900–800 cm^{-1}, respectively.[42] Furthermore, the vibrational modes of the H_2O molecules appear in the range of 3200 to 3500 cm^{-1} and at 1646 cm^{-1}, which are related to the bending, symmetric, and asymmetric stretching of the H–O–H bonds, respectively. In addition, the O–H stretching mode of $H_2PO_4^-$ appeared as three A, B, and C bands at about 3100–3200 cm^{-1} (A band), 2300–2400 cm^{-1} (B band), and 1600–1800 cm^{-1} (C band).[43]

2.5.3. ^{31}P-MAS-NMR spectroscopy. Solid-state ^{31}P NMR was performed to investigate the coordination of phosphorus species (PO_4^{3-}) in the prepared samples (Fig. 4). The ^{31}P MAS NMR spectrum of hydroxyapatite shows an isotopic signal at 1.94 ppm, indicating the presence of a phosphorus group (PO_4^{3-}) in the prepared HAP. Similarly, HAP-S1 showed a narrow isotopic signal at 1.82 ppm, indicating that the sample contained one type of phosphorus group, and this shift can be explained by the change in the global environment of PO_4^{3-} after acid treatment. It should be noted here that the possible presence of a tiny amount of non-rigid HPO_4^{2-} was not manifested by a separate signal. In fact, the non-discrete HPO_4^{2-} exhibited an isotropic shift that overlaps with that of HAP, as described by Rothwell *et al.*[44] Moreover, the spectrum of HAP-S2 shows the presence of an intense peak at 2.22 ppm, which can be attributed to PO_4^{3-} of the apatite.[44] However, the spectrum shows an additional non-intense band at −1.63 ppm, which can be attributed to PO_4^{3-} in the formed $CaHPO_4$ phase.[44] Furthermore, the presence of small upfield peaks could be attributed to the heterogeneity of the environment. However, cross-polarisation (CP) at low temperature could be applied to enhance the multinuclear signal intensities.[44,45]

CP ^{31}P-NMR was performed on the HAP-S3 sample, as shown in Fig. 5, revealing the presence of several signals. The interpretation of the spectrum of HAP-S3 requires sufficient caution due to the overlapping of these signals. Considering the complexity of these results and the high sensitivity of this technique to the presence of P in the sample, the intense peak at 3.1 ppm can be attributed to the possible presence of orthophosphate group residues of $Ca_{10}(PO_4)_6(OH)_2$.[46] The overlap of a small peak with the previous HAP-associated signal at −1.46 ppm followed by an intense signal at 1.50 and a non-symmetric signal at 5.77 ppm may be attributed to the presence of $Ca(H_2PO_4)_2 \cdot H_2O$ and the possible existence of acidic phosphate residues such as $CaHPO_4$, $CaHPO_4 \cdot 2H_2O$, and $Ca(H_2PO_4)$, which could be precipitated during the complex dissolution–precipitation process of the apatite in highly acidic medium.[47,48] Furthermore, the possible substitution of orthophosphate in the calcium sulfate crystals can also be a possible reason, which may explain the multiple signals detected.

2.5.4. Scanning electron microscopy. The surface morphology of the prepared materials is shown in Fig. 6. According to the SEM images, the morphology of the prepared HAP shows heterogeneous microstructure particles. After acid treatment, crystallites with different forms were observed for HAP-S1. A further increase in the acid concentration led to a change in the particle forms and the formation of agglomerated blocks.

The surface elemental analysis of the prepared samples by energy dispersive spectroscopy is presented in Table 2.

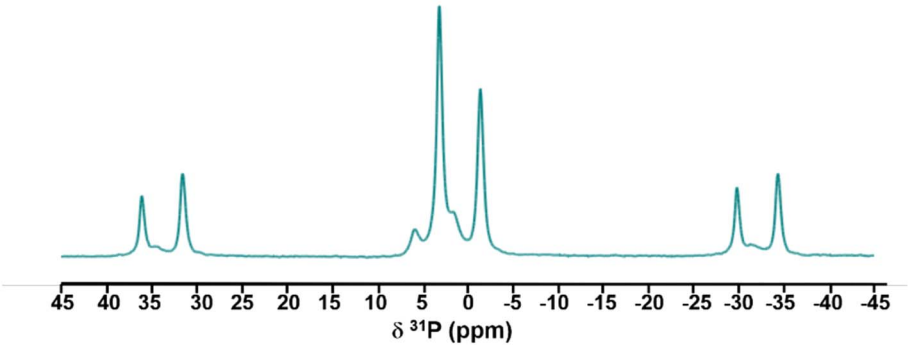

Fig. 5 CP ^{31}P-NMR spectrum of the HAP-S3 sample.

According to the results, the materials are mainly composed of Ca, P and O for all the samples, besides the presence of sulfur for HAP-S1, HAP-S2 and HAP-S3. In fact, the Ca and P contents decreased slightly after the treatment of apatite in acid medium. However, the sulfur content increased with an increase in the sulfonic acid concentration.

2.5.5. Elemental mapping. As shown by the elemental mapping in Fig. 7, the distribution of Ca, P and O elements varied from each sample depending on the sulfonic acid treatment. In the case of HAP-S1, HAP-S2 and HAP-S3, the sulfur distribution was found to be homogeneous over the selected zone. Therefore, the sulfur content was found to be more concentrated in the HAP-S3 surface. According to these figures, it can clearly be concluded that the materials are mainly composed of Ca, O, S and P elements, which are homogeneously and regularly distributed over their surface.

3. Catalytic investigation in esterification, transesterification and two-step process

3.1. Oleic acid esterification investigation

3.1.1. Effect of heating mode and catalyst screening. To investigate the effect of microwave irradiation and the prepared materials on the catalytic activity of the esterification progress, preliminary experiments were conducted in a stainless-steel batch reactor without MW irradiation using a methanol to oleic acid molar ratio of 8 : 1 and catalyst amount of 7 wt% at 150 °C for 60 min as control experiments (Fig. 8). The first experiment was conducted without any catalyst, resulting in the production of 6.5% OAME. Under similar conditions, in the presence of HAP, HAP-S1, HAP-S2 and HAP-S3, yields of 11%, 30.9%, 38.6%, and 48%, respectively, were obtained. This

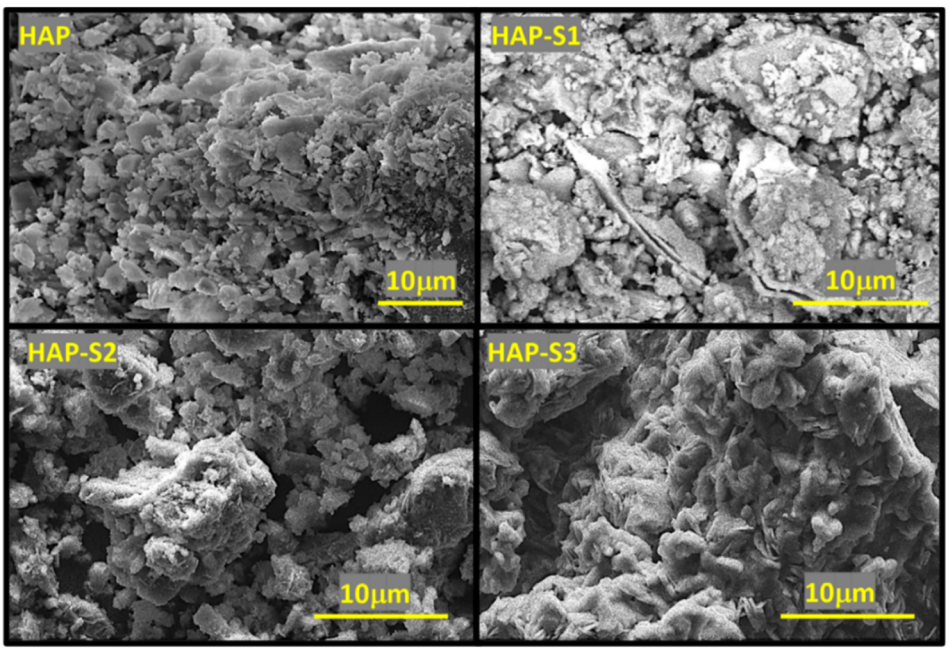

Fig. 6 SEM micrographs of the prepared materials.

Table 2 Surface elemental analysis of the prepared materials using EDX

	Element content (wt%)				
Material	Ca	P	O	S	C
HAP	42.71	18.4	35.36	—	3.53
HAP-S1	40.84	16.27	34.19	6.47	2.23
HAP-S2	36.62	14.61	41.97	11.02	1.21
HAP-S3	27.86	7.20	50.57	14.37	—

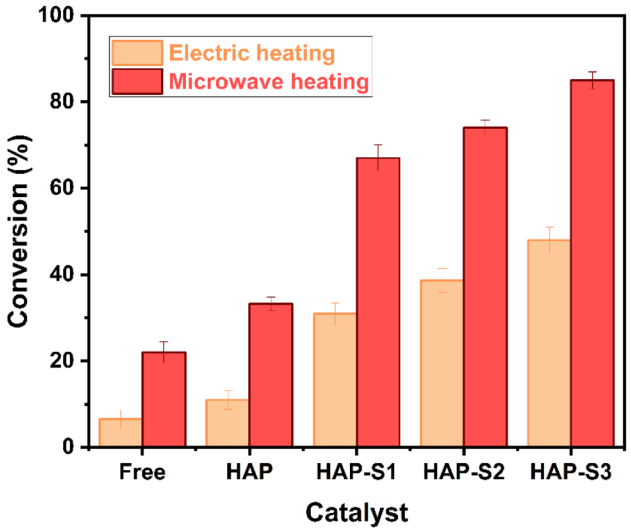

Fig. 8 Effect of heating mode on OAME yield over the prepared materials (conditions: methanol to oleic acid molar ratio of 8 : 1 and catalyst amount of 7 wt% at 150 °C for 60 min).

enhancement in the obtained yield is due to the presence of active sites in the surface of the utilized materials. We observed that higher concentrations of sulfonic acid-treated HAP resulted in an increase in the acidity of the catalyst, which enhanced its catalytic activity by providing more active sites for the reaction. Nevertheless, we believe that better results can be obtained by conducting these reactions for longer durations. In fact, the majority of the reviewed works that carried out the esterification of OA in batch reactors required more rigorous reaction conditions to obtain high biodiesel yields, high molar ratios of alcohol-to-oil, and also presented longer reaction times than that used in the present tests.[12,49] Alternatively, performing the same experiments under MW irradiation (Fig. 8) resulted in higher yields compared to that obtained by the heated stainless-steel batch reactor, confirming the beneficial effect of MW. In particular, an oleic acid conversion of 22% was obtained with the free catalytic system, whereas 33.2%, 67%, 74% and 85% was obtained using HAP, HAP-S1, HAP-S2 and HAP-S3, respectively. In fact, in electrically assisted heating, the heat energy is transferred from the surface to the reactor by convection and conduction. Therefore, a large amount of heat and long reaction time are required to achieve the satisfactory conversion of fatty acids to FAME. In contrast, microwave irradiation can deliver the energy directly to the reactants which enhances the heat transfer due to the interaction of the dipole moment of the polar methanol with the incident radiation. Actually, the role of microwave irradiation is pivotal in accelerating the reaction rates. The ability of microwaves to provide uniform heating and enhance the mass transfer leads to faster reaction kinetics

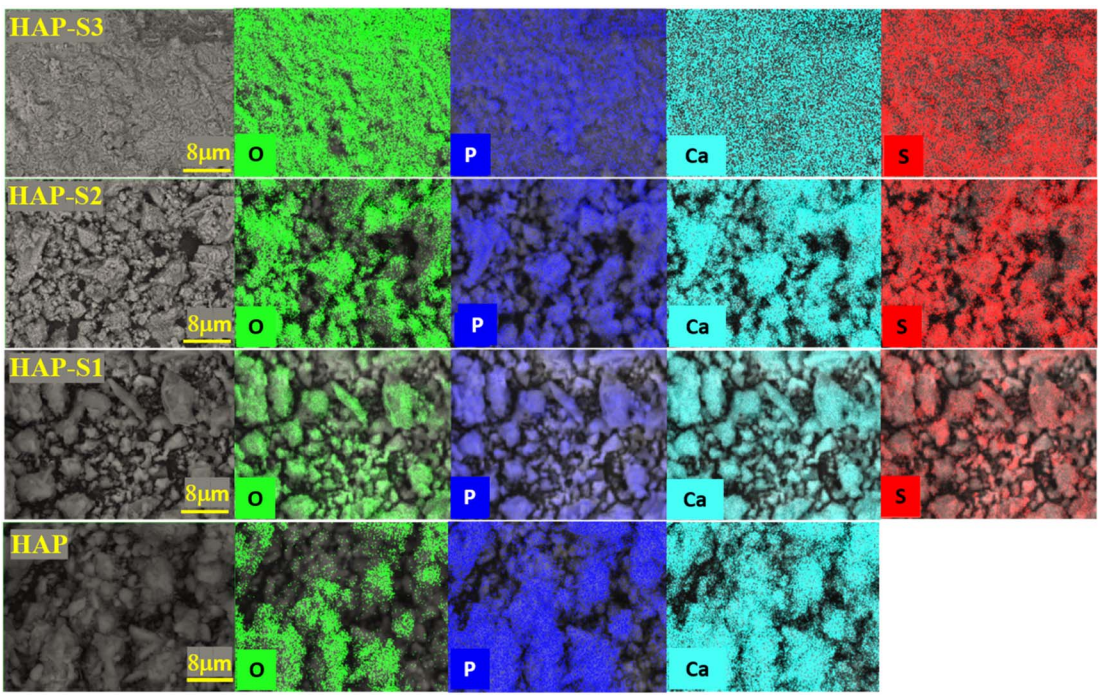

Fig. 7 Elements mapping (O, P, Ca and S) of the prepared materials.

compared to conventional heating methods. The interaction between radiation and dipole moment of methanol results in the rotation, friction and collision of molecules, resulting in instantaneous localized superheating, where high energy is delivered to the reagents at a very fast rate. Here, the reaction mixture was rapidly heated when exposed to MW irradiation and formed hot spots, known as the "microwave thermal effect", which is responsible for the increased reaction efficiency.[50]

3.1.2. Leaching test. Subsequently, we studied the leaching of the prepared catalysts using the half-time filtration test. Specifically, after 10 min of reaction under the pre-optimized reaction conditions, the catalysts were separated from the reaction medium by centrifugation, and then the obtained liquid was reintroduced into the tube and subjected to a new run for another 30 min. HAP-S1 showed the lowest leaching, where the homogeneous contribution was negligible and found to be 3.3%. Therefore, in the following sections, the HAP-S1 catalyst was selected as the optimal catalyst for the esterification of oleic acid with methanol, given that it contains active SO_3H groups in the esterification process.

3.1.3. Study of the effect of reaction parameters. To determine the dependence of the oleic acid esterification on the reaction conditions, the effects of different parameters were investigated. Firstly, the effect of reaction temperature on the oleic acid conversion under MW was studied by varying the reaction temperature in the range of 100–150 °C, as shown in Fig. 9a, while keeping the other factors constant (catalyst loading of 7 wt%, methanol to acid molar ratio of 8 : 1 and reaction time of 60 min). The oleic acid conversion was found to increase with an increase in temperature due to the higher molecular collisions between the reagents as a result of the improved mass transfer, which increased the reaction rate.[51] To investigate the effect of the catalyst amount on the esterification conversion, different amounts of catalyst ranging from 5 to 12 wt% were used, while keeping the other experimental conditions constant. Based on the results obtained (Fig. 9b), the conversion increased as the catalyst amount increased from 5 to 10 wt%. Therefore, the catalyst amount of 10 wt% was selected as the optimum value given that further increasing the catalyst amount to 12 wt% resulted in an OA conversion increase of only 6.45% with a final total value of 80%. In general, increasing the catalyst amount increased the number of available catalytic acid active sites responsible for promoting the esterification process. The effect of the molar ratio of methanol to acid was also studied. In fact, the stoichiometric ratio of methanol to oleic acid for esterification is defined as one. However, to drive the reaction equilibrium towards ester production, an excess amount of methanol is recommended.[12] As shown in Fig. 9c, the yield of methyl oleates increased from 65.1% to 85.47% by increasing the molar ratio from 6 : 1 to 10 : 1, while keeping the other parameters constant. However, the conversion remained constant with a further increase in the molar ratio to 12 : 1. The reaction duration was varied from 10 to 60 min in the presence of 7 wt% of HAP-S1 catalyst and the optimal methanol to acid molar ratio of 10 : 1. As shown in Fig. 9d, the conversion

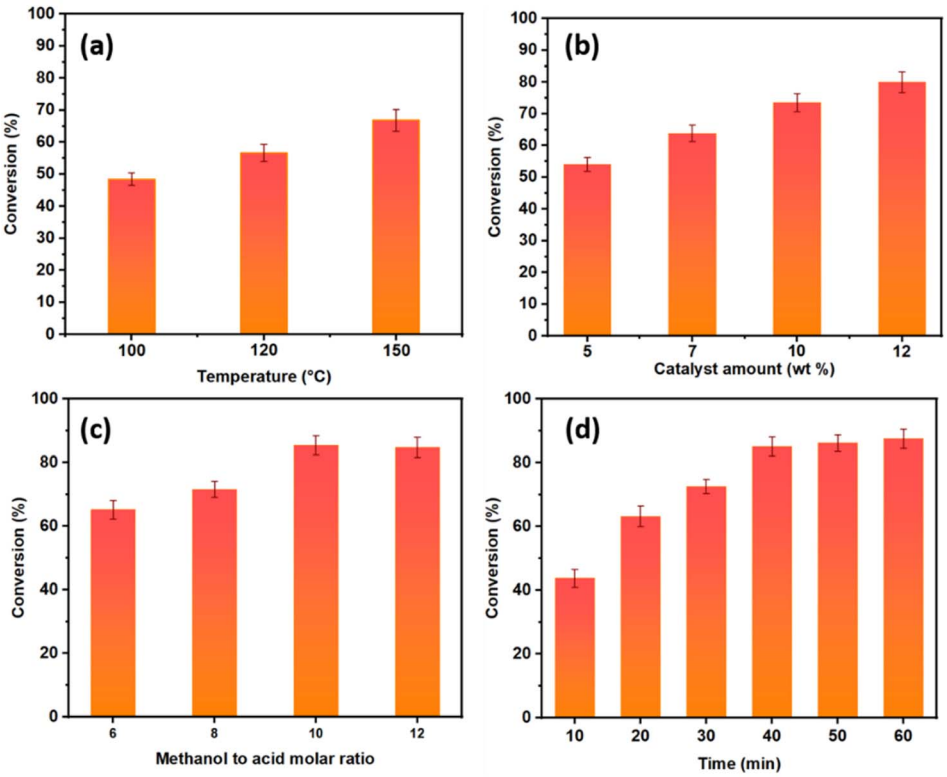

Fig. 9 Effect of reaction conditions on oleic acid conversion: (a) effect of reaction temperature, (b) effect of catalyst amount, (c) effect of the methanol to acid molar ratio and (d) effect of reaction time.

increased with the prolongation of the reaction time. After 10 min of reaction under MW irradiation, a yield of 42.75% was obtained. Increasing the reaction time to 40 min resulted in a methyl oleate yield of 85%. Thus, this duration was determined to be the optimal reaction time. Therefore, it should be noted that in general, the catalytic performances are also related to the strength and density of the catalytic sites.[32,52]

3.1.4. Quantitative characterization of OAME by ^{1}H-NMR. The esterification of oleic acid to methyl oleate was estimated using the reported acid–base titrimetric method. In general, the results obtained are similar to that determined using ^{1}H-NMR spectroscopy. Here, after completion of the reaction under the optimized conditions, the obtained product was analysed by both acid–base titration and ^{1}H-NMR spectroscopy and found to be 85.4% and 87%, respectively. The ^{1}H-NMR spectrum of oleic acid and the obtained methyl oleate after dilution in $CDCl_3$ is shown in Fig. 10.

As shown, the typical triplets of the oleic acid methylene group (α-CH2) adjacent to the carbonyl group are present in the oleic acid spectrum at 2.34–2.37 ppm. Under the optimal conditions, the spectrum of methyl oleate revealed the presence of new characteristic peaks, with a triplet appearing at 2.30–2.33 ppm assigned to the (α-CH_2) of methyl oleate, and these signals appeared at a chemical shift lower than that of (α-CH_2) of the carboxylic group due to their deshielding effect. In fact, the intensities of these triplets are proportional to the concentration of each molecule in the final product. In addition, a new intense singlet appeared at 3.67 ppm, which is attributed to the protons of the methoxy group (R–O–CH_3) of the methyl esters.

3.1.5. Qualitative characterization of OAME by FTIR. The qualitative analysis of methyl oleate by FTIR is shown in Fig. 11. The peaks at 2780 and 2970 cm^{-1} show the symmetric and antisymmetric stretching vibrations of C–H in the CH_2 and CH_3 groups, respectively, in both spectra. The peaks at 1600–1400 cm^{-1} confirm the bending vibrations of the CH_2 and CH_3 aliphatic groups. The intense peak at 1711 cm^{-1} is attributed to the C=O carbonyl groups present in the carboxyl group of oleic acid, and the intense peak at 1739 cm^{-1} confirms the stretching vibration of C=O present in the esters.

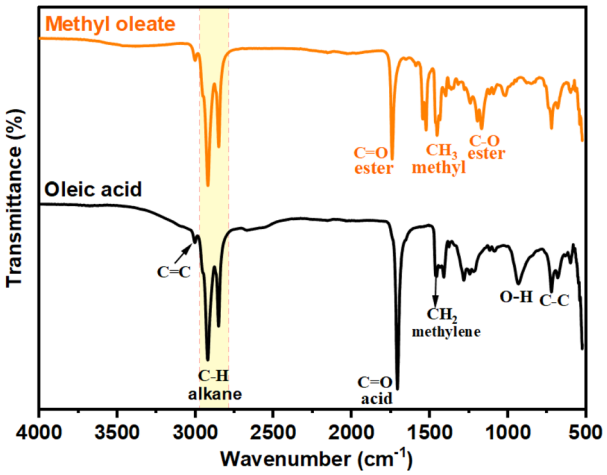

Fig. 11 FTIR spectra of oleic acid and methyl oleates.

3.2. Possible esterification mechanism

The esterification process is the combination of an organic acid with an alcohol to form an ester. From a mechanistic point of view, the esterification process is a catalytic nucleophilic acyl substitution that occurs based on the nature of electrophilicity of the carbon atom of carbonyl and the nucleophilicity of the alcohol. Based on this information, we propose a reasonable mechanism for the esterification reaction over the HAP-S1 catalyst. In fact, two plausible mechanisms can be proposed according to the literature because there are two different active sites in the active sulfonic group, S=O and S–O–H, as described by Vafaeezadeh and Fattahi[53] and Dou *et al.*[54] Therefore, we hypothesize that the reaction process probably follows a dual-site mechanism, in which two separate SO_3H groups are involved in the reaction pathway, as shown in the Scheme 1. Firstly, the interaction of the oleic acid carbonyl with the Brønsted acid site (S–O–H group) of the catalyst surface leads to the formation of a carbocation (electro-deficient carbon of the acid). Similarly, the adsorption of the adjacent Lewis acid site (S=O group) *via* the hydroxyl oxygen leads to the formation of an h-bonded alcohol molecule, which attacks the protonated carbonyl group to form a tetrahedral intermediate. Subsequently, internal rearrangement, followed by the elimination of a water molecule from the obtained intermediate results in the production of methyl oleates (Scheme 1).

3.2.1. Reusability. To study the reuse and acid site stability of the catalyst, the sulfonated hydroxyapatite was separated

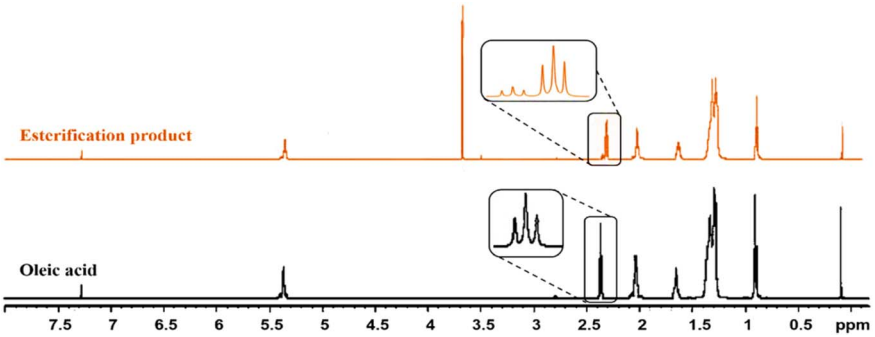

Fig. 10 ^{1}H-NMR spectra of oleic acid and the obtained product after esterification.

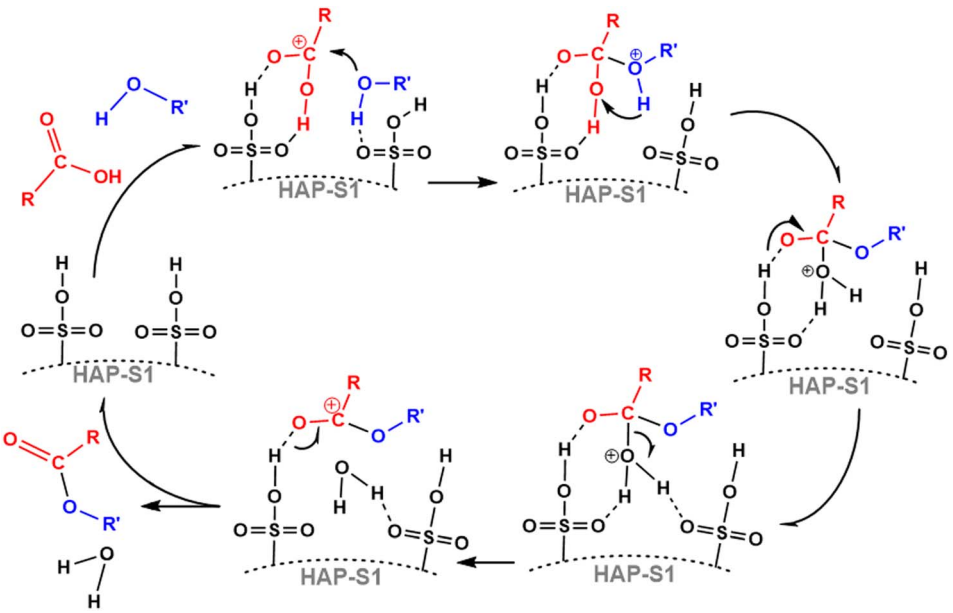

Scheme 1 Proposed mechanism of the acid-catalyzed esterification reaction.

from the reaction medium by centrifugation, washed with ethanol, dried at 80 °C and used for the next cycle. The yields of methyl oleates were found to be 80%, 72% and 60% after three cycles, respectively. It is widely reported that leaching of the sulfonic groups is a common problem, which is the probable reason for the decrease in catalytic activity after catalyst reuse and its possible deactivation by reaction with methanol to form sulfonate esters, as reported by Fraile *et al.*[55]

3.3. Transesterification of rapeseed oil

The results obtained for the rapeseed oil transesterification indicate that a conversion of only 17.6% was achieved after 40 min of reaction. Alternatively, for a longer reaction time of 60 min, the conversion reached 40.2%. Thus, based on the obtained results, the acid sulfonated apatite could promote the conversion of vegetable oil. However, the kinetic rate was found to be lower than that of the base-catalyzed process. In general, acid-catalyzed transesterification is not widely applied due to the requirement of catalysts with a high total acid site density,[32] high alcohol to oil molar ratio, longer reaction time and additional energy to achieve high yields.[56–58] Therefore, the majority of sulfonated acid catalysts are evaluated for the esterification of free fatty acids.

3.4. Double-step esterification/transesterification of acidic oil

After the successful application of the selected acid catalyst in the esterification of oleic acid and its potential application in the transesterification reaction, we aimed to study it in the esterification of FFA-containing oils to investigate the ability of the catalyst to perform simultaneous esterification and transesterification reactions. In this context, a mixture of rapeseed oil with 5 wt% oleic acid was prepared and used as a model feedstock for the production of biodiesel from a low-cost feedstock. The initial acid value of the feedstock was found to be 15.26 mg KOH per g. Esterification was carried out under the optimized conditions for 60 min. At the end of the reaction, the catalyst was separated by centrifugation and the excess methanol was evaporated by rotary evaporation. Based on the titration method, the acid value was determined to be 7.5 mg KOH per g. The catalyst could reduce the acidity of the original feedstock by 50.85%. The evaporated ester phase containing the remaining FFA, untransesterified triglycerides, diglycerides and monoglyceride was introduced in a second MW-driven reaction, in which 10 wt% of fresh catalyst was added in addition to an amount of methanol equal to that introduced in the first step. The final product exhibited an acid value of 3.1 mg KOH per g, and thus the total FFA conversion after the two-step reaction

Table 3 Product acid values and FAME yields before and after the two-step process

	First step	Second step	
Feedstock's initial acid value (mg KOH per g)	First reaction acid value (mg KOH per g)	Second reaction acid value (mg KOH per g)	Total FAME yield (%)
15.26	7.5	3.11	40.13

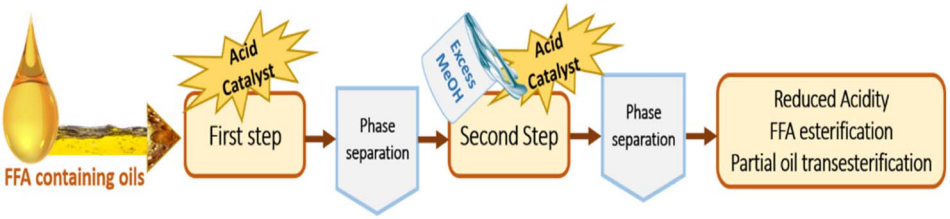

Fig. 12 Double-step esterification/transesterification of acidic oil.

Table 4 Comparison with reported catalysts for oleic acid esterification under microwave irradiation

Entry	Catalyst	Time (min)	T (°C)	Catalyst amount (wt%)	Methanol/oleic acid	Methyl oleate yield (%)	Reference
1	HAP-S1	40	150	10	10 : 1	87	This work
2	Sulfated zirconia	20	200	5	10 : 1	68.7	65
3	Nb_2O_5	20	200	5	10 : 1	68	65
4	I-ISS-300	30	120		10 : 1	93	66
5	[Bmim]HSO_4	30	120	10	9 : 1	84.7	67
6	H_2SO_4	30	120	10	9 : 1	87.7	67
7	Wasted flint kaolin	40	115	—	60 : 1	96.5	68
8	UiO-66-SO_3H	60	100	8	20 : 1	98.3	69

was 79.6% (according to titration results) with a total FAME production of 40.13% (Table 3), as determined by ^{1}H-NMR according to the method reported in the literature.[34,59] In fact, the competitive FFA esterification and TG transesterification by the acid catalytic sites and the possible hydrolysis of TG by the generated water may limit the total biodiesel yield.[32,60] Also, the reaction mechanisms of the two pathways are different given that the methanolysis of FFAs proceeds *via* simple esterification, while TGs proceed *via* transesterification, which involves several consecutive steps.[61] A relevant aspect should also be noted, where the achieving high yields by simultaneous esterification/transesterification is related to the strength of the catalytic sites and their high surface density, in addition to the further optimization of the reaction parameters, which can play an important role increasing the conversion.[52]

Based on these results, it can be concluded that the HAP-S1 catalyst is a potential solid acid catalyst for FFA removal from acidic feedstocks. Consequently, given that the acid value of the final product was less than 4 mg KOH per g after two reaction runs, it is recommended to adopt an alkali-catalyzed transesterification to increase the biodiesel yield and achieve the ester value required by ASTM and EN 14214.[19,62–64] A summary of the two-step process adopted is shown in Fig. 12.

3.5. Comparison with reported catalysts for the microwave-assisted esterification of oleic acid under

To allow a proper comparison with the results obtained herein, the data of the relevant works published in the literature dealing with the microwave-assisted esterification of oleic acid for biodiesel are presented in Table 4. The synthesized catalyst showed competitive catalytic activity with respect to other catalytic systems such as sulfated zirconia, Nb_2O_5, sulfonated silica I-ISS-300, waste flint kaolin, MOF-based catalyst UiO-66-SO_3H, ionic liquid [Bmim]HSO_4 and homogeneous H_2SO_4 catalyzed system. Moderate alcohol to acid molar ratios were reported for entries 2 to 6, but high molar ratios were required (for 7 and 8) to achieve the optimal conversion of OA to OAME.

4. Conclusion

In this study, hydroxyapatite-derived natural phosphate was prepared *via* the dissolution–precipitation of natural Moroccan phosphate in nitric acid. Subsequently, the hydroxyapatite was treated with chlorosulfonic acid in dichloromethane at three acidity levels. Specifically, the HAP-S1 material was investigated in the oleic acid esterification, resulting in an optimal oleic acid methyl ester yield of 87% after 40 min of reaction under microwave irradiation. This confirmed the synergistic influence between microwave irradiation and the prepared catalyst. Also, the catalyst was tested in the transesterification reaction of rapeseed oil, but the final yield was found to be lower than that of the esterification reaction, given that a lower transesterification rate was observed. Furthermore, the catalyst was found to be a potential catalyst for the esterification of FFA-containing feedstocks, given that it could reduce the FFA content of acidified rapeseed oil as a model of a low-quality feedstock after a two-step process. However, the extra purity of the acid used and the meticulous preparation procedure may affect the catalyst preparation procedure and increase the overall cost of catalyst preparation, despite the abundance of the apatite source in Morocco. Thus, further research should be conducted to evaluate the energetic and economic aspects of the developed material for the synthesis of biodiesel.

Data availability

Data for this article, including (material characterisation and conversion results) are available from the corresponding

author, Dr Boutaina REZKI. All collected data are present in the paper as figures or tables. The data can be requested from the corresponding author.

Author contributions

Boutaina Rezki: conceptualization, investigation, data curation, methodology, formal analysis, writing original draft, writing – review & editing. Younes Essamlali: formal analysis, visualization, validation. Othmane Amadine: provided help for biodiesel analysis realization. Said Sair: SEM-mapping analysis for the materials. Mina Aadil: co-supervision. Mohamed Zahouily: project administration, supervision, validation, writing – review & editing and resource.

Conflicts of interest

The authors declare that there are no conflicts of interest to declare.

Acknowledgements

Authors express their gratitude to the University of Hassan II of Casablanca in Morocco. Authors also thank the Moroccan Foundation for Advanced Science, Innovation and Research (MAScIR) – UM6P for characterization facilities. Dr Boutaina Rezki express special thanks to Dr Oussama Oulhakem, Dr Abdallah Nayad, Dr Az-Eddine El Mansouri and Dr Dalia Allouss for their assistance.

References

1 R. Vitiello, F. Taddeo, V. Russo, R. Turco, A. Buonerba, A. Grassi, *et al.*, Production of Sustainable Biochemicals by Means of Esterification Reaction and Heterogeneous Acid Catalysts, *ChemEngineering*, 2021, **5**, 1–14.

2 N. Z. Abdul Kapor, G. P. Maniam, M. H. A. Rahim and M. M. Yusoff, Palm fatty acid distillate as a potential source for biodiesel production-a review, *J. Cleaner Prod.*, 2017, **143**, 1–9, DOI: **10.1016/j.jclepro.2016.12.163**.

3 H. A. Farag, A. El-maghraby and N. A. Taha, Optimization of factors affecting esterification of mixed oil with high percentage of free fatty acid, *Fuel Process. Technol.*, 2011, **92**, 507–510, DOI: **10.1016/j.fuproc.2010.11.004**.

4 P. Saxena, S. Jawale and M. H. Joshipura, A review on prediction of properties of biodiesel and blends of biodiesel, *Procedia Eng.*, 2013, **51**, 395–402, DOI: **10.1016/j.proeng.2013.01.055**.

5 R. N. Vilas-Bôas, L. Lucchetti, L. D. Fernandes, M. A. S. da Costa and M. F. Mendes, Preparation and Utilization of Hydroxyapatite-Supported Na and CaO–CeO2 Catalysts for Biodiesel Production Using Vegetable Oil Deodorization Distillate as Raw Material, *Catal. Lett.*, 2023, **153**, 2456–2470, DOI: **10.1007/s10562-022-04173-2**.

6 I. Atadashi, M. Aroua, A. A. Aziz and N. M. Sulaiman, The effects of catalysts in biodiesel production: A review, *J. Ind. Eng. Chem.*, 2013, **19**, 14–26, DOI: **10.1016/j.jiec.2012.07.009**.

7 P. C. Duarte, F. Carvalho Ballotin, H. Limborço, J. Domingos Ardisson, R. Montero Lago and C. T. Ana Paula de, Heterogeneous acid catalyst based on sulfated iron ore tailings for oleic acid esterification, *Appl. Catal., A*, 2020, **600**, 117624, DOI: **10.1016/j.apcata.2020.117624**.

8 S. Soltani, U. Rashid, I. Arbi Nehdi and S. Ibrahim Al-Rasayes, Esterification of Palm Fatty Acid Distillate Using a Sulfonated Mesoporous CuO-ZnO Mixed Metal Oxide Catalyst, *Chem. Eng. Technol.*, 2017, 1–10, DOI: **10.1002/ceat.201700138**.

9 L. Tumkot, A. T. Quitain, P. Boonnoun, N. Laosiripojana, T. Kida and A. Shotipruk, Synergizing Sulfonated Hydrothermal Carbon and Microwave Irradiation for Intensified Esterification Reaction, *ACS Omega*, 2020, **5**, 23542–23548, DOI: **10.1021/acsomega.0c01660**.

10 S. Zhang, Y. Zu, Y. Fu, M. Luo, D. Zhang and T. Efferth, Rapid microwave-assisted transesterification of yellow horn oil to biodiesel using a heteropolyacid solid catalyst, *Bioresour. Technol.*, 2010, **101**, 931–936, DOI: **10.1016/j.biortech.2009.08.069**.

11 N. Narkhede, S. Singh and A. Patel, Recent Progress on Supported Polyoxometalates for Biodiesel Synthesis via Esterification and Transesterification, *Green Chem.*, 2015, **17**, 89–107, DOI: **10.1039/C4GC01743A**.

12 Y. Essamlali, M. Larzek, B. Essaid and M. Zahouily, Natural phosphate supported titania as a novel solid acid catalyst for oleic acid esterification, *Ind. Eng. Chem. Res.*, 2017, **56**, 5821–5832, DOI: **10.1021/acs.iecr.7b00607**.

13 R. Chakraborty and D. Roychowdhury, Optimization of biological-hydroxyapatite supported iron catalyzed methyl oleate synthesis using response surface methodology, *J. Taiwan Inst. Chem. Eng.*, 2013, **45**, 92–100, DOI: **10.1016/j.jtice.2013.05.006**.

14 R. Chakraborty and D. Roychowdhury, Fish bone derived natural hydroxyapatite-supported copper acid catalyst: Taguchi optimization of semibatch oleic acid esterification, *Chem. Eng. J.*, 2013, **215–216**, 491–499, DOI: **10.1016/j.cej.2012.11.064**.

15 J. V. Ruatpuia, G. Halder, S. Mohan, B. Gurunathan, H. Li, F. Chai, *et al.*, Microwave-assisted biodiesel production using ZIF-8 MOF-derived nanocatalyst: A process optimization, kinetics, thermodynamics and life cycle cost analysis, *Energy Convers. Manage.*, 2023, **292**, 117418, DOI: **10.1016/j.enconman.2023.117418**.

16 V. K. Mishra and R. Goswami, A review of production, properties and advantages of biodiesel, *Biofuels*, 2017, **9**, 273–289, DOI: **10.1080/17597269.2017.1336350**.

17 Q. Chen, A. Wang, W. Quan and W. Gang, Efficient synthesis of biodiesel from Hyoscyamus niger L. seed oil by base catalysis, *Fuel Process. Technol.*, 2023, **241**, 107630, DOI: **10.1016/j.fuproc.2022.107630**.

18 S. Elias, A. M. Rabiu, B. I. Okeleye, V. Okudoh and O. Oyekola, Bifunctional Heterogeneous Catalyst for Biodiesel Production from Waste Vegetable Oil, *Appl. Sci.*, 2020, **10**, 3153, DOI: **10.3390/app10093153**.

19 B. Rezki, Y. Essamlali, M. Aadil, N. Semlal and M. Zahouily, Biodiesel production from rapeseed oil and low free fatty

acid waste cooking oil using a cesium modified natural phosphate catalyst, *RSC Adv.*, 2020, **3**, 41065–41077, DOI: 10.1039/d0ra07711a.

20 I. Cacciotti, Cationic and Anionic Substitutions in Hydroxyapatite, *Handbook of Bioceramics and Biocomposites*, 2016, pp. 145–211, DOI: 10.1007/978-3-319-12460-5.

21 B. Rezki, Y. Essamlali, O. Amadine, S. Sair, M. Aadil, C. Len, *et al.*, A comprehensive review on apatite-derived catalysts for sustainable biodiesel production: Classification, features and challenges, *J. Environ. Chem. Eng.*, 2024, **12**, 111913, DOI: 10.1016/j.jece.2024.111913.

22 A. El Mansouri, A. Oubella, M. Maatallah, M. Y. Aititto, M. Zahouily, H. Morjani, *et al.*, Design, synthesis, biological evaluation and molecular docking of new uracil analogs-1,2,4-oxadiazole hybrids as potential anticancer agents, *Bioorg. Med. Chem. Lett.*, 2020, **30**, 127438, DOI: 10.1016/j.bmcl.2020.127438.

23 H. Yook, J. Hwang, W. Yeo, J. Bang, J. Kim, T. Y. Kim, *et al.*, Design Strategies for Hydroxyapatite-Based Materials to Enhance Their Catalytic Performance and Applicability, *Adv. Mater.*, 2022, **35**, 1–36, DOI: 10.1002/adma.202204938.

24 I. El yaakouby, I. Rhrissi, Y. Abouliatim, M. Hlaibi and N. Kamil, Moroccan sardine scales as a novel and renewable source of heterogeneous catalyst for biodiesel production using palm fatty acid distillate, *Renewable Energy*, 2023, **217**, 119223, DOI: 10.1016/j.renene.2023.119223.

25 L. Ma'mani, M. Sheykhan, A. Heydari, M. Faraji and Y. Yamini, Sulfonic acid supported on hydroxyapatite-encapsulated-γ-Fe2O3 nanocrystallites as a magnetically Brønsted acid for N-formylation of amines, *Appl. Catal., A*, 2010, **377**, 64–69, DOI: 10.1016/j.apcata.2010.01.020.

26 M. Mamaghani, Z. Taati, M. Rasoulian, J. Yousefizad, N. Toraji, M. Mohsenimehr, *et al.*, [γ-Fe2O3@HAp-SO3H] an efficient nanocatalyst for the synthesis of highly functionalised 2-thioxopyrido[2,3-d]pyrimidines, *J. Chem. Res.*, 2016, **40**, 29–34, DOI: 10.3184/174751916X14495860660659.

27 K. F. Sina, A. Yahyazadeh, N. O. Mahmoodi, K. R. Moghadam, M. Nikpassand and M. Rasa, Ultrasonic Assisted Synthesis of 2, 3-Dihydroquinazolin-4(1H)-ones Involving Three-Component Reaction of Isatoic Anhydride, Amines and Pyrazole Carbaldehydes Catalyzed by [ɣ-Fe2O3@HAp-SO3H], *Lett. Org. Chem.*, 2020, **17**, 24–30, DOI: 10.2174/1570178616666190401183953.

28 J. Deng, L.-P. Mo, F.-Y. Zhao, L.-L. Hou, L. Yang and Z.-H. Zhang, Sulfonic acid supported on hydroxyapatite-encapsulated -γ-Fe2O3 nanocrystallites as a magnetically separable catalyst for one-pot reductive amination of carbonyl compounds, *Green Chem.*, 2011, **13**, 2576–2584, DOI: 10.1039/c1gc15470b.

29 N. Yousefi and S. Batool, Sulfonated nanohydroxyapatite functionalized with 2-aminoethyl dihydrogen phosphate (HAP@AEPH2-SO3H) as a reusable solid acid for direct esterification of carboxylic acids with alcohols, *Res. Chem. Intermed.*, 2016, **42**, 5789–5806, DOI: 10.1007/s11164-015-2404-8.

30 V. Akubude, K. Jaiyeoba, T. Oyewusi, E. Abbah, J. Oyedokum and V. Okafor, *Overview on Different Reactors for Biodiesel Production*, 2021, pp. 341–59.

31 S. Nomanbhay and M. Yin Ong, A Review of Microwave-Assisted Reactions for Biodiesel Production, *Bioengineering*, 2017, **4**, 1–21, DOI: 10.3390/bioengineering4020057.

32 S. Chellappan, K. Aparna, C. Chingakham, V. Sajith and V. Nair, Microwave assisted biodiesel production using a novel Brønsted acid catalyst based on nanomagnetic biocomposite, *Fuel*, 2019, **246**, 268–276, DOI: 10.1016/j.fuel.2019.02.104.

33 S. El Asri, A. Laghzizil, A. Saoiabi, A. Alaoui, K. El Abassi, R. M'hamdi, *et al.*, A novel process for the fabrication of nanoporous apatites from Moroccan phosphate rock, *Colloids Surf., A*, 2009, **350**, 73–78, DOI: 10.1016/j.colsurfa.2009.09.006.

34 L. A. Anderson and A. K. Franz, Real-Time Monitoring of Transesterification by 1 H NMR Spectroscopy: Catalyst Comparison and Improved Calculation for Biodiesel Conversion, *Energy Fuels*, 2012, **26**, 6404–6410.

35 K. C. V. Kumar, T. J. Subha, K. Ahila, B. Ravindran, S. Chang, A. H. Mahmoud, *et al.*, Spectral characterization of hydroxyapatite extracted from Black Sumatra and Fighting cock bone samples : A comparative analysis, *Saudi J. Biol. Sci.*, 2020, **28**, 840–846, DOI: 10.1016/j.sjbs.2020.11.020.

36 S. Dorozhkin, Dissolution mechanism of calcium apatites in acids: A review of literature, *World J. Methodol.*, 2012, **2**, 1–17, DOI: 10.5662/wjm.v2.i1.1.

37 S. O. Nur, U. Rashid, M. Sufri Mastuli and Y. Hin Taufiq-Yap, Esterification of palm fatty acid distillate (PFAD) to biodiesel using bi-functional catalyst synthesized from waste angel wing shell (Cyrtopleura costata), *Renewable Energy*, 2019, **131**, 187–196, DOI: 10.1016/j.renene.2018.07.031.

38 M. Zarghani and B. Akhlaghinia, Sulfonated nanohydroxyapatite functionalized with 2-aminoethyl dihydrogen phosphate (HAP@AEPH2-SO3H) as a new recyclable and eco-friendly catalyst for rapid one-pot synthesis of 4,4′-(aryl methylene)bis(3-methyl-1H-pyrazol-5-ol)s, *RSC Adv.*, 2015, **5**, 87769–87780, DOI: 10.1039/c5ra16236j.

39 Å. Bengtsson and S. Sjöberg, Surface complexation and proton-promoted dissolution in aqueous apatite systems, *Pure Appl. Chem.*, 2009, **81**, 1569–1584, DOI: 10.1351/PAC-CON-08-10-02.

40 R. Jahanshahi and B. Akhlaghinia, Sulfonated Honeycomb Coral (HC-SO3H): a new, green and highly efficient heterogeneous catalyst for the rapid one-pot bis (3-methyl-1H-pyrazol-5-ol)s, *Chem. Pap.*, 2017, **71**, 1351–1364, DOI: 10.1007/s11696-016-0127-y.

41 A. Oulguidoum, H. Bouyarmane, A. Laghzizil, J. Nunzi and A. Saoiabi, Development of sulfonate-functionalized hydroxyapatite nanoparticles for cadmium removal from aqueous solutions, *Colloid Interface Sci. Commun.*, 2019, **30**, 100178, DOI: 10.1016/j.colcom.2019.100178.

42 S. Seesanong, C. Seangarun, B. Boonchom, N. Laohavisuti, K. Chaiseeda and W. Boonmee, Composition and Properties of Triple Superphosphate Obtained from Oyster

Shells and Various Concentrations of Phosphoric Acid, *ACS Omega*, 2021, **6**, 22065–22072, DOI: 10.1021/acsomega.1c02660.

43 B. Boonchom, Parallelogram-like microparticles of calcium dihydrogen phosphate monohydrate (Ca(H2PO4)2·H2O) obtained by a rapid precipitation route in aqueous and acetone media, *J. Alloys Compd.*, 2009, **482**, 199–202, DOI: 10.1016/j.jallcom.2009.03.157.

44 W. P. Rothwell, J. Waugh and J. P. Yesinowskit, High-Resolution Variable-Temperature 31P NMR of Solid Calcium Phosphates, *J. Am. Chem. Soc.*, 1980, **102**, 2637–2643.

45 B. Louati, F. Hlel, K. Guidara and M. Gargouri, Analysis of the effects of thermal treatments on CaHPO4 by 31P NMR spectroscopy, *J. Alloys Compd.*, 2005, **394**, 13–18, DOI: 10.1016/j.jallcom.2004.10.025.

46 S. Verma and R. Murugavel, Di-tert-butylphosphate Derived Thermolabile Calcium Organophosphates: Precursors for Ca(H2PO4)2, Ca(HPO4), α-/β-Ca(PO3)2, and Nanocrystalline Ca10(PO4)6(OH)2 Sonam, *Inorg. Chem.*, 2020, **59**, 13233–13244, DOI: 10.1021/acs.inorgchem.0c01591.

47 Y. Wang, M. Tang, A. Yusuf, Y. Wang, X. Zhang, G. Yang, *et al.*, Preparation of Catalyst from Phosphorous Rock Using an Improved Wet Process for Transesterification Reaction, *Ind. Eng. Chem. Res.*, 2021, **60**, 8094–8107, DOI: 10.1021/acs.iecr.1c01072.

48 C. Chen, H. Zheng, S. Tang, T. Zhang and L. Lv, Study on Controlling the Dissolution of Calcium Dihydrogen Phosphate Using Ternary Phase Diagrams to Improve the Production Process of Phosphoric Acid, *Ind. Eng. Chem. Res.*, 2022, **61**(43), 15970–15979, DOI: 10.1021/acs.iecr.2c03146.

49 P. Yin, L. Chen, Z. Wang, R. Qu, X. Liu, Q. Xu, *et al.*, Biodiesel production from esterification of oleic acid over aminophosphonic acid resin D418, *Fuel*, 2012, **102**, 499–505, DOI: 10.1016/j.fuel.2012.05.027.

50 C. A. R. Melo-Júnior, C. E. R. Albuquerque, M. Fortuny, C. Dariva, S. Egues, A. F. Santos, *et al.*, Use of microwave irradiation in the noncatalytic esterification of C18 fatty acids, *Energy Fuels*, 2009, **23**, 580–585, DOI: 10.1021/ef800766x.

51 L. Tumkot, A. T. Quitain, P. Boonnoun, N. Laosiripojana, T. Kida and A. Shotipruk, Synergizing sulfonated hydrothermal carbon and microwave irradiation for intensified esterification reaction, *ACS Omega*, 2020, **5**, 23542–23548, DOI: 10.1021/acsomega.0c01660.

52 S. Chellappan, V. Nair, V. Sajith and K. Aparna, Experimental validation of biochar based green Bronsted acid catalysts for simultaneous esterification and transesterification in biodiesel production, *Bioresour. Technol. Rep.*, 2018, 28–44, DOI: 10.1016/j.biteb.2018.04.002.

53 M. Vafaeezadeh and A. Fattahi, DFT investigations for "Fischer" esterification mechanism over silica-propyl-SO3H catalyst: is the reaction reversible?, *Comput. Theor. Chem.*, 2015, **1071**, 27–32, DOI: 10.1016/j.comptc.2015.07.028.

54 Y. Dou, H. Zhang, A. Zhou, F. Yang, L. Shu, Y. She, *et al.*, Highly efficient catalytic esterification in a -SO3H functionalized Cr(III)-MOF, *Ind. Eng. Chem. Res.*, 2018, **57**, 8388–8395, DOI: 10.1021/acs.iecr.8b01239.

55 J. M. Fraile, E. García-bordejé and L. Roldán, Deactivation of sulfonated hydrothermal carbons in the presence of alcohols: Evidences for sulfonic esters formation, *J. Catal.*, 2012, **289**, 73–79, DOI: 10.1016/j.jcat.2012.01.017.

56 J. A. Melero, L. F. Bautista, G. Morales, J. Iglesias and D. Briones, Biodiesel Production with Heterogeneous Sulfonic Acid-Functionalized Mesostructured Catalysts, *Energy Fuels*, 2009, **23**, 539–547.

57 V. Mandari and S. K. Devarai, Biodiesel Production Using Homogeneous, Heterogeneous, and Enzyme Catalysts via Transesterification and Esterification Reactions: a Critical Review, *BioEnergy Res.*, 2021, **15**, 935–961, DOI: 10.1007/s12155-021-10333-w.

58 M. Chai, Q. Tu, M. Lu and Y. J. Yang, Esterification pretreatment of free fatty acid in biodiesel production, from laboratory to industry, *Fuel Process. Technol.*, 2014, **15**, 106–113.

59 G. Gelbard, O. Br, R. M. Vargas, F. Vielfaure and U. E. Schuchardt, 1H Nuclear Magnetic Resonance Determination of the Yield of the Transesterification of Rapeseed Oil with Methanol, *J. Am. Oil Chem. Soc.*, 1995, **72**, 1239–1241.

60 N. Boz, N. Degirmenbasi and D. M. Kalyon, Esterification and Transesterification of Waste Cooking Oil over Amberlyst 15 and Modified Amberlyst 15 Catalysts, *Appl. Catal., B*, 2014, **165**, 723–730, DOI: 10.1016/j.apcatb.2014.10.079.

61 S. Martinez Luz, R. Romero, R. Natividad and J. González, Optimization of biodiesel production from sunflower oil by transesterification using Na2O/NaX and methanol, *Catal. Today*, 2014, **220–222**, 12–20, DOI: 10.1016/j.cattod.2013.08.022.

62 R. Sheikh, M. Choi, J. Im and Y. Park, Study on the solid acid catalysts in biodiesel production from high acid value oil, *J. Ind. Eng. Chem.*, 2013, **19**, 1413–1419, DOI: 10.1016/j.jiec.2013.01.005.

63 A. D. Ogunsola, M. O. Durowoju, A. O. Alade, S. O. Jekayinfa and O. Ogunkunle, Modeling and optimization of two-step shea butter oil biodiesel synthesis using snail shells as heterogeneous base, *Energy Adv.*, 2022, **1**, 113–128, DOI: 10.1039/d1ya00042j.

64 S. Niju, F. Raj Russell, C. Anushya and M. Balajii, Optimization of acid catalyzed esterification and mixed metal oxide catalyzed transesterification for biodiesel production from Moringa oleifera oil, *Green Process. Synth.*, 2019, **8**, 756–775.

65 C. A. R. Melo Junior, C. E. R. Albuquerque, S. A. C. Juliana, C. Dariva, M. Fortuny, A. F. Santos, *et al.*, Solid-Acid-Catalyzed Esterification of Oleic Acid Assisted by Microwave Heating, *Ind. Eng. Chem. Res.*, 2010, **49**, 12135–12139.

66 Z. Hasan, J. W. Yoon and S. H. Jhung, Esterification and acetylation reactions over in situ synthesized mesoporous

sulfonated silica, *Chem. Eng. J.*, 2014, **278**, 105–112, DOI: 10.1016/j.cej.2014.12.025.

67 S. Bölük and Ö. Sönmez, Microwave-Assisted Esterification of Oleic Acid using an Ionic Liquid Catalyst, *Chem. Eng. Technol.*, 2020, **43**, 1–19, DOI: 10.1002/ceat.202000045.

68 A. D. O. Nazaré, L. Rafaela da Silva Costa, L. Helena de Oliveira Pires, L. S. d. N. Adriano, R. Angélica, E. F. d. C. Carlos, *et al.*, Microwave-assisted preparation of a new esterification catalyst from wasted flint kaolin, *Fuel*, 2013, **103**, 626–631, DOI: 10.1016/j.fuel.2012.07.017.

69 G. S. Prasad, K. Ngaosuwan, S. Assabumrungrat, M. Selvaraj, G. Halder and S. Lalthazuala Rokhum, Microwave assisted biodiesel production using sulfonic acid-functionalized metal-organic frameworks UiO-66 as a heterogeneous catalyst, *Renewable Energy*, 2022, **197**, 161–169.